NRC Research Press

ARTICLE

Microfacies and microstructures of subglacial and deglacial sediments from the Pingualuit Crater Lake (Ungava Peninsula, Canada)

Hervé Guyard, Pierre Francus, Guillaume St-Onge, Sonja Hausmann, and Reinhard Pienitz

Abstract: The Pingualuit Crater (Ungava Peninsula, Canada) hosts a freshwater basin in which a subglacial lake subsisted under the Laurentide Ice Sheet during the last glacial period. Microfacies and microstructures of a 9 m long sediment core are presented to discuss the depositional environment of deformed glacigenic and postglacial sequences deposited in the deep basin of the lake. Five distinct lithofacies are characterized. The range of glacial microstructures observed in the lower facies (Facies IV) reveals that high stress level occurred outside the crater during the formation of this diamicton released by the ablation of debris-rich basal glacier ice in an ice contact subglacial–proglacial lacustrine environment. The overlying subaqueous and glacigenic sediment gravity flow (Facies IIIb) is associated with a temporary absence of ice cover over the coring site, and likely results from the efflux plume and the associated suspension sedimentation produced during the retreat of the ice margin. Then, the finely laminated (<1–2 mm) and normally graded meltout silts (Facies IIIa) containing dropstones and load cast features suggest underflows in an unstable ice marginal lacustrine environment hydrologically separated from the retreating glacier but containing floating glacial ice blocks. Microstructures within occasional diamictic layers indicate sudden meltout deposits from these drifting ice blocks. The above finer-grained sediments (Facies Ib) lack typical glacial microstructures, marking the onset of postglacial organic sedimentation. These postglacial sediments are affected by post-depositional deformations due to an overlying rotational slide (Facies II) that may have perturbed the associated environmental record.

Résumé : Le cratère des Pingualuit (Péninsule d'Ungava, Canada) abrite un bassin d'eau douce dans lequel un lac sous-glaciaire a subsisté sous la calotte laurentidienne pendant la dernière période glaciaire. Les microfaciès et microstructures sédimentaires d'une carotte de 9 m prélevée dans le bassin profond sont présentés pour discuter des environnements de dépôt associés aux sédiments déformés glaciogéniques et post-glaciaires. Cinq lithofaciès sont caractérisés. Les microstructures glaciaires du faciès en base de carotte (Facies IV) révèlent un haut niveau de stress pendant la formation en dehors du cratère de ce diamicton libéré par l'ablation basale du glacier dans un environnement lacustre sous-glaciaire/proglaciaire. Le dépôt sus-jacent, résultant d'un courant gravitaire de sédiments glaciogéniques (Facies IIIb), reflète un environnement temporairement libre de glace au site de carottage et résulte probablement du panache d'écoulement produit pendant le retrait du front glaciaire. Puis, les fines rhythmites (<1–2 mm) silteuses, normalement granoclassées et contenant des « dropstones » et des figures de charge (Facies IIIa) suggèrent des courants de fond dans un environnement glacio-lacustre marginal et instable, séparé hydrologiquement du glacier en retrait mais renfermant des blocs de glace. Les microstructures de couches diamictiques occasionnelles indiquent des dépôts soudains liés à la fonte de ces blocs dérivants. Les sédiments organiques sus-jacents (Facies Ib), à grains plus fins et caractérisés par l'absence de microstructures glaciaires, marquent ensuite le début de la période postglaciaire. Le facies présente des déformations post-sédimentaires liées au dépôt par-dessus d'un glissement rotationnel (Facies II) qui a pu perturber l'enregistrement environnemental associé.

Introduction

Within the last decades, micromorphological studies have been applied to a wide range of sedimentary settings (e.g., van der Meer and Menzies 2011) to determine the sediment origin and depositional environment (Seret 1993; Lachniet et al. 2001; Menzies and Zaniewski 2003; Phillips et al. 2007; Kilfeather et al. 2010; van der Meer et al. 2010). Micromorphological techniques within glacial sediments have become a common procedure to differentiate individual lithofacies types occurring within glacial subenvironments, to investigate the often complex and long-term history of the sediments (Lachniet et al. 2001; Menzies and Zaniewski 2003; Carr et al. 2006; Phillips et al. 2007; Menzies and Whiteman 2009; Rémillard et al. 2013), and to study subglacial processes because glacigenic sediments present microstructures related to stress histories (Menzies and Maltman 1992; van der Meer 1993; Hiemstra and van der Meer 1997; Menzies 1998; van der Wateren et al. 2000; Hiemstra and Rijsdijk 2003; Larsen et al. 2007). These studies out-

Received 28 February 2014. Accepted 23 July 2014.

Paper handled by Associate Editor Timothy Fisher.

H. Guyard. Institut des sciences de la mer de Rimouski (ISMER), Université du Québec à Rimouski, Rimouski, QC G5L 3A1, Canada; GEOTOP Research Center, Montréal, QC H3C 3P8, Canada; Laboratoire Géosciences Paris-Sud (GEOPS), UMR CNRS 8148, Université Paris-Sud 11, Orsay, France.
P. Francus. GEOTOP Research Center, Montréal, QC H3C 3P8, Canada; Centre Eau Terre Environnement, Institut National de la Recherche Scientifique, Québec, QC G1K 9A9, Canada.
G. St-Onge. Institut des sciences de la mer de Rimouski (ISMER), Université du Québec à Rimouski, Rimouski, QC G5L 3A1, Canada; GEOTOP Research Center, Montréal, QC H3C 3P8, Canada.
S. Hausmann. Academy of Natural Sciences of Drexel University, Patrick Center for Environmental Research, Philadelphia, PA 19103, USA.
R. Pienitz. Centre d'études nordiques (CEN) & Département de Géographie, Université Laval, QC G1V 0A6, Canada.
Corresponding author: Hervé Guyard (e-mail: herve.guyard@u-psud.fr).

Fig. 1. Location and photographs (from Guyard et al. 2011) of the Pingualuit Crater Lake in the northernmost Ungava Peninsula (Canada) showing the isolation of the basin (i.e., no surface connection to other surrounding water bodies) and its steep and boulder-strewn internal walls (upper panel). Lower panel illustrates a digital elevation model and glacial landforms mapped in the area by Daigneault (1997), as well as the regional main glacial flow directions (large black arrows) following Bouchard and Marcotte (1986). Dashed grey line delimits the present shores of Lake Laflamme and the white dot indicates the coring site. U, Ungava flow; P, Payne flow.

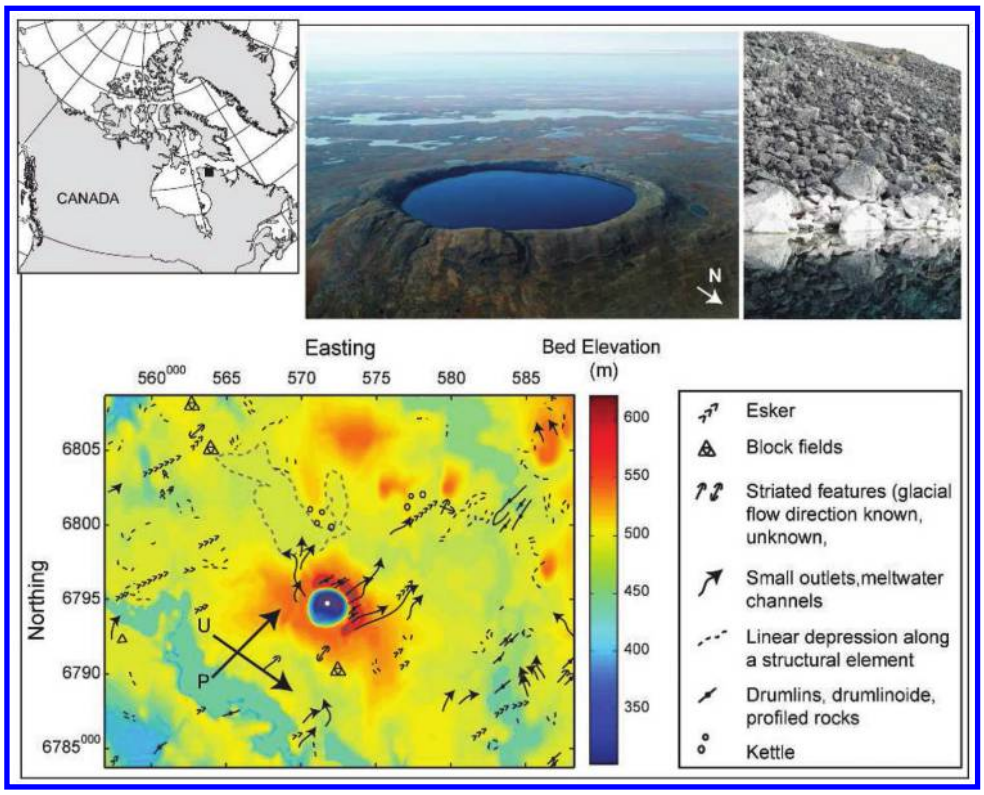

lined that the formation, (post) depositional processes, and stress history of sediments can only be adequately discussed when studying the assemblages of the individual glacial microstructures. Moreover, the examination of microstructures within sediment gravity flow deposits has not only revealed possible destruction of the features present in the source sediments and the development and preservation of sediment flow-related structures, but also important similarities with subglacial sediments (Lachniet et al. 1999, 2001; Menzies and Zaniewski 2003).

In this study, the micromorphology of the Pingualuit Crater Lake (Ungava Peninsula, Canada; Fig. 1) sediments is examined. This site offers the opportunity to explore sedimentary processes occurring within subglacial lakes, which are poorly known environments despite the recent discovery of numerous and active Antarctica subglacial lakes and their influence on ice sheet dynamics (Bell et al. 2007; Wingham et al. 2006; Wright and Siegert 2012). Indeed, because of its geographic position, its morphometry (shape and depth), and its age, the lake was covered by the Laurentide Ice Sheet (LIS) while escaping erosion (cf. Bouchard 1989; Guyard et al. 2011). Chronostratigraphic and classical sedimentological and multiproxy analyses on a 9 m long core retrieved in the deep basin of the lake (244 m water depth) were previously described and used to investigate the paleoenvironmental conditions during the Late Pleistocene (Guyard et al. 2011; Black et al. 2012; Luoto et al. 2013). This sedimentary sequence reflects the transition from subglacial to postglacial conditions in a lacustrine environment within the context of the last deglaciation. Here we present the microstructures of the glacigenic and postglacial sediments from thin sections to (*i*) contribute to the inventory of microstructures observed in glacigenic and sediment flow deposits in subglacial lakes, and (*ii*) refine the interpretation of other paleoenvironmental indicators preserved in this unusual setting, hence improving the environmental reconstruction of this unique record.

Setting and background

The Pingualuit Crater (61°17′N, 73°40′W, Canada; Fig. 1) resulted from a meteoritic impact ca. 1.4 Ma (Grieve et al. 1991) and forms an almost perfectly circular depression about 410 m deep and 3.4 km in diameter, hosting an extremely transparent, dilute ultraoligotrophic lake presently 246 m deep and 2.8 km in diameter (Bouchard 1989). It is one of the most transparent lakes on the planet (Gantner et al. 2011), as it is only fed by precipitation. The Pingualuit Crater Lake also has a very limited littoral zone due to its steep basin walls (26°–35°) and boulder-strewn slopes (Fig. 1). The maximum altitude of the rim is 657 m a.s.l., which is one of the highest summits in Ungava Peninsula (Fig. 1). It rises to 163 m above the present lake surface and 120 m above the surrounding terrain. The crater was affected by at least two distinct glacial movements, the Payne and the Ungava flows, but the surrounding area presents numerous glacial landforms mainly in the direction of the Payne flow (Fig. 1), considered as the main and sustained glacial flow during the last glaciation (Daigneault and Bouchard 2004). Geomorphological features in the crater area indicate glacial retreat from northeast to southwest (e.g., Bouchard 1989). The crater was one of the last areas of the ice sheet in the Ungava Peninsula to become ice-free (Dyke and Prest 1987; Lauriol and Gray 1987). In addition, due to the favorable morphometry of the crater (shape and depth) and to its geographical location near former centers of successive North American ice sheets, the deep basin sediments likely escaped glacial erosion and would thus represent a unique long-term archive in the terrestrial Canadian Arctic (Bouchard 1989; Pienitz et al. 2009). Glacial modeling of the

hydraulic potential confirmed the possibility of the persistence of a subglacial lake at least during the last glacial maximum under the LIS (Guyard et al. 2011). Indeed, the high fluid pressures modeled at the rock–ice interface around the basin combined with the morphometry of the depression suggest storage of subglacial water within the crater (Guyard et al. 2011). Yet, the relatively small size of the Pingualuit subglacial basin should have limited the development of necessary gradients to drive sufficient circulation within the reservoir (e.g., Tikku et al. 2005). The subglacial crater is thus unlikely to be analogous, for example, to the much larger Lake Vostok (Studinger et al. 2004) or to former subglacial lakes existing under the LIS (Evatt et al. 2006; Livingstone et al. 2012).

In the Northern Hemisphere, the retreat of the LIS has exposed a number of settings containing subglacial lake sediments. Sedimentary processes within these former and much larger subglacial lakes under the LIS, such as the Subglacial Lake McGregor (Munro-Stasiuk 2003) and the Great Slave Lake (Christoffersen et al. 2008), include gravity flow, water transport, suspension settling, and underflows. Sedimentary facies in subglacial lakes are likely to be characterized by a complex succession of meltout of debris-rich basal ice and subaqueous debris flow deposits (see Bentley et al. 2011 and Livingstone et al. 2012 for a review) and can be used to track changes in the subglacial environment mainly linked to changing glacier dynamics and mass transport and indirectly to climate change (e.g., Hodgson et al. 2009).

The Pingualuit Crater Lake is strongly affected by mass movement events, as revealed by recent geophysical surveys of the lake basin (Ledoux et al. 2011; Desiage 2014). The upper 9 m of an at least 150 m thick sedimentary sequence (Bouchard 1989) was retrieved from the deep basin of the lake and divided into six distinct lithofacies (Fig. 2) as described in Guyard et al. (2011) using geochemical, magnetic, and physical properties of the sediments. The base of the core (Facies IV) consists of the uppermost part of a very dense diamicton deposited in an ice-contact subglacial–proglacial lake with permanent thin ice cover by basal meltout and marking the end of subglacial conditions. The overlying sediments (Facies IIIb and Facies IIIa) likely reflect the hydrological separation of the lake from the retreating glacier and indicate various ice cover conditions. Within these glacigenic units, infrared stimulated luminescence and accelerator mass spectrometry ^{14}C dating of bulk sediments, as well as biostratigraphic data, indicate sediment mixing between recent (e.g., Holocene) and much older (pre- to mid-Wisconsinan) material reworked by glacier activity (Guyard et al. 2011). This process prevents the precise dating of these sediments that were deposited just before the final deglaciation of the lake (Fig. 2). The onset of organic sediments (Facies Ib) dated at ca. 6850 cal years BP traduces the onset of the postglacial ice-free period and the inception of lacustrine productivity associated with the final disappearance of the last remnant of the ice sheet (Black et al. 2012; Luoto et al. 2013). Finally, a large mass wasting deposit (MWD, Facies II) affecting the entire deep basin separates the postglacial (Facies Ib) and Late Holocene (Facies Ia) organic sediments (Fig. 2). This MWD is also clearly seen on the seismic records of the lake (Guyard et al. 2011; Desiage 2014).

Materials and methods

Sediment cores (Fig. 2) were retrieved from the deepest part of the lake (244 m water depth; 61°16′46.5″N, 73°39′44.7″W; Fig. 1) using the UWITEC gravity and percussion piston coring system. U-channels were sampled in the center of the short gravity (surface) and long piston cores and run through a CAT-scan at INRS-ETE (Quebec City) with a pixel resolution of 0.1 mm. Images were processed with MATLAB software to map X-ray attenuation coefficients on longitudinal images and to visualize sedimentary structures. The resulting images are displayed in a greyscale with the darker grey representing a lower X-ray attenuation (Boespflug et al. 1995; Guyard et al. 2007*a*). Greyscale values are expressed as CT numbers, which are complex units related to the mineralogy, organic matter content, grain size, and bulk density (e.g., Fortin et al. 2013).

Fig. 2. General and simplified lithostratigraphy of the cores retrieved in the deep basin of the lake and lithofacies, modified from Guyard et al. (2011) and Luoto et al. (2013). (1) Angular lithified centimetre-scale clasts (dropstones), (2) organic-rich clayey silts, (3) cross-laminations, (4) large folds and deformations, (5) muddy sand intervals, (6) inclined and normal graded laminations in inorganic sandy silt intervals, (7) horizontal and normal graded laminations in inorganic sandy silt intervals, (8) compact, light clay layer.

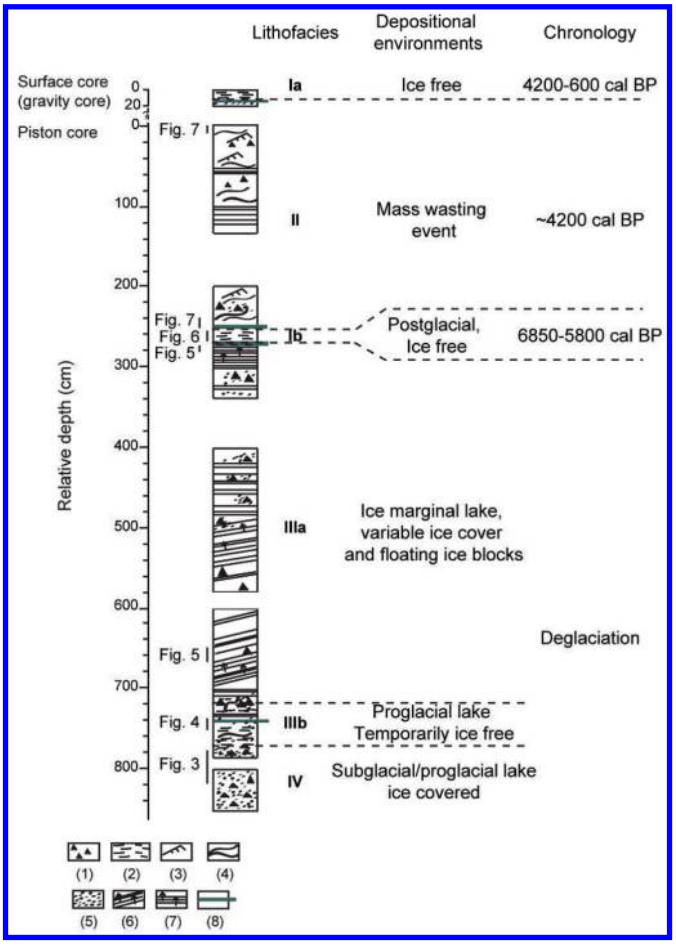

Decimetre long sediment slabs were removed from the split core sections at chosen intervals in each facies (Fig. 2) using an electro-osmotic cutter to prevent smearing due to high clay content (Francus and Cosby 2001). The slabs were then freeze dried and impregnated with Spurr's low viscosity epoxy resin (Lamoureux 1994). They were placed under low vacuum (90 kPa) until the sediment was saturated with resin and cured at 70 °C. No carbonates are present in the watershed (Daigneault and Bouchard 2004) nor in the sediments (Guyard et al. 2011). Thin sections were digitized at 2400 dpi (pixel size = 10.6 μm) with a flatbed transparency scanner. Specific regions of interest within thin sections were examined using a Zeiss Evo 50 scanning electron microscope in backscattered electron mode, which optimizes contrast between clastic grains and sedimentary plasma (1 pixel = 1 μm). Microphotographs were also taken from the thin sections using a petrographic microscope at INRS-ETE under both plane and cross-polarized light at low magnifications. Intervals with recognizable perturbations related to coring and subsampling (e.g., injection structures, laboratory-induced voids) were not detected

Table 1. Glossary of recurrent micromorphological terms according to van der Meer (1993).

Domains	Zones of sediment with unique textural characteristics that can be distinguished from the surrounding sediment.
Grain lineations	Arrangement of elongated skeleton grains. The preferred orientation of grains is developed by grain rotation and aligned within discrete shear zones. Can be single or multiple (cross-cutting single lineations). Commonly found in sediment subjected to stress, such as subglacial till and debris flow deposits.
Matrix	All material smaller than the thickness of the thin section. Individual particles can therefore not be distinguished. Also called plasma.
Plasmic fabric	Arrangement of birefringent, optically aligned plasma domains only visible under cross-polarized light. Also called b-fabric in soil sciences. Below are some common patterns of plasmic fabric, depending on the optical characteristics of plasma particles and on their arrangement between each other.
Masepic plasmic fabric	Short plasma domains mainly oriented in a single preferred orientation.
Lattisepic plasmic fabric	Short and discontinuous plasma domains oriented approximately in two perpendicular directions. This pattern is often associated with a skelsepic arrangement.
Skelsepic plasmic fabric	Birefringent plasma domains oriented parallel to the surface of skeleton grains.
Kinking plasmic fabric	Characterized by "tiger skin" pattern of extinction bands often seen in individual lenses of clay-rich material and oriented to each other at high angles. The dominant preferred orientation between extinction bands is more or less at a right angle.
Pressure shadow	Symmetric or asymmetric tails of concentrated fine material on both sides of larger grains. Rarely observed completely in thin sections because of the sample fabrication. Indicative of planar shearing (symmetric) or rotation (asymmetric).
Skeleton (grain) or S-matrix	Single grain larger than the thickness of a thin section.
Turbate/galaxy structure	Circular alignment of relatively fine grains occurring both with and without a core stone. Due to rotational movement.

and are unlikely to induce misinterpretations (Stow and Aksu 1978).

Micromorphology provides an insight into both individual clastic material (i.e., skeleton grains or S-matrix, >35 μm in size; Table 1) and surrounding ground mass (i.e., plasma, <25–30 μm in size) and their mutual geometric arrangement and structural attributes (van der Meer 1993). Microstructures and microfabrics, representing the sediment internal architecture, can be linked to plasma (i.e., plasmic fabric), to the S-matrix, or to both plasma and S-matrix (e.g., van der Meer and Menzies 2011). The description using qualitative observations follows the pedological nomenclature established by Brewer (1976) and the glossary of micromorphological terms supplied by van der Meer (1993). A glossary of recurrent micromorphological terms is also given in Table 1.

Results: micromorphological descriptions

Facies IV

Facies IV is characterized by unsorted and bimodal coarse sediments (Figs. 2, 3). The plasma consists of silt and clay. Skeleton grains range from 35 μm to 5 mm, with a dominant grain size of 200 μm. Roundness (see Krumbein 1941) is medium to high for large grains, while smaller grains are often more angular. The spatial distribution of skeleton grains is relatively homogeneous and ranges from closed to single spaced to close porphyric, i.e., skeleton clasts are in contact or separated by a distance equivalent to their size (Stoops and Jongerius 1975). No grading was detected in the samples. Porosity is always less than 10%. Multiple diamicton domains, many turbate structures, both with and without core stones, clast halo, and discrete shear lines are visible, as well as linear features formed by the spatial arrangement of particles (Figs. 3A, 3B**).** Edge to edge crushed grains and crushed grains are common features (Figs. 3D, 3F). The three types of edge to edge crushed grains (microcracks, flakes, and transgranular fractures) identified by Rawling and Goodwin (2003) were recognized (Fig. 3D). The upper thin section of this facies also contains elongated and subangular mud pebbles composed of homogeneous fine material (pebble type III; van der Meer 1993) **(**Fig. 3E). The fine material is rarely diffusely reoriented in domains. When observed, the patterns are the skelsepic (parallel to skeleton grain surfaces) and lattisepic (cross striated) plasmic fabrics.

Facies IIIb

Facies IIIb shows a dominance of silt and clay (Figs. 2, 4). Skeleton grains are rarely present and float in a continuous mass of fine material (i.e., open porphyric distribution; Stoops and Jongerius 1975). Their distribution is heterogeneous and sometimes zonal (e.g., Fig. 4D). Their size ranges from 50 μm to 2 mm, with a dominance of the 100 μm fraction. Some skeleton grains are very well rounded, while the majority of them have relatively low rounding and medium to high angularity. The influence of water is evident throughout this facies. A "comet" structure, a common microstructure in glacial sediments, is observed in water-influenced fine-grained plasma (Fig. 4A), as well as fluid escape structures (Fig. 4C), rare and isolated rotational structures (Figs. 4C, 4F), and clast haloes (Fig. 4H). Relatively homogeneous fine sandy beds surrounded by alternating fine silts and clay layers with a pod form (Fig. 4G) or showing several tails (Fig. 4E) are detected. Load cast due to large rock fragment are detected and resulted in the disturbance of the sandy bed. A masepic pattern of phyllosilicates reorientation (plasmic fabric) is sometimes visible (Fig. 4B), as well as banded and mottled plasma (Fig. 4D). High angle extinction bands within short birefringent plasma domains (Fig. 4G) may reflect a "kinking" plasmic fabric (van der Meer 1993).

Facies IIIa

While Facies IIIa is apparently homogeneous at a macroscopic level, thin section microphotographs and backscattered electron images reveal that the sediment is in fact bedded, as well as finely and rhythmically laminated (Fig. 5). In the lower part of this facies (Fig. 2), most laminations are highly inclined and distinctly normally graded, mainly from fine sand or silt to clays (Fig. 5A). They range in thickness from less than 100 μm to 1–2 mm. The boundary between a fine-grained unit and the next coarse-grained unit is generally sharp. Occasionally, the coarse unit may be restricted to a single grain layer, with the grains themselves being sometimes dispersed. Isolated >1 mm sand grains are also observed. In this environment, they correspond to outsized clasts and are considered as dropstones (Fig. 5B). In this facies, load casting, as well as rolling features, are also common (Figs. 5C, 5D) and are occasionally at the origin of postdepositional folds in the underlying and (or) overlying laminae. Inverse synsedimentary faults affecting only a

Fig. 3. Left panel: Flatbed scan of thin sections of Facies IV with corresponding regions of interest (ROI). Middle and right panels: (A) Microphotograph and (A′) associated sketch showing multiple diamicton domains, skeleton grain, plasma lineation (ln), and turbate structures (ts). Porosity is defined by planar voids (vo). Cross-polarized light. (B) Microphotograph and (B′) associated sketch of turbate structure (ts) around "core stones" (cs). Note the pressure shadow below the clast (black arrow), multiple diamicton domains and skeleton grain and plasma lineations (ln). Plane light. (C) Silt and clay coating around a large skeleton grain and forming a halo (delimited by white dashed line). Cross-polarized light. (D) Some crushed grains and types of edge to edge crushed grains: microcracks (m), transgranular fractures (t), and flakes (f). Plane light. (E) Mud pebbles (white arrows) containing an internal plasmic fabric and encircled by voids that are easily distinguished from the surrounding diamicton (type III pebble; van der Meer, 1993). Cross-polarized light. (F) Edge to edge crushed grains. Plane light.

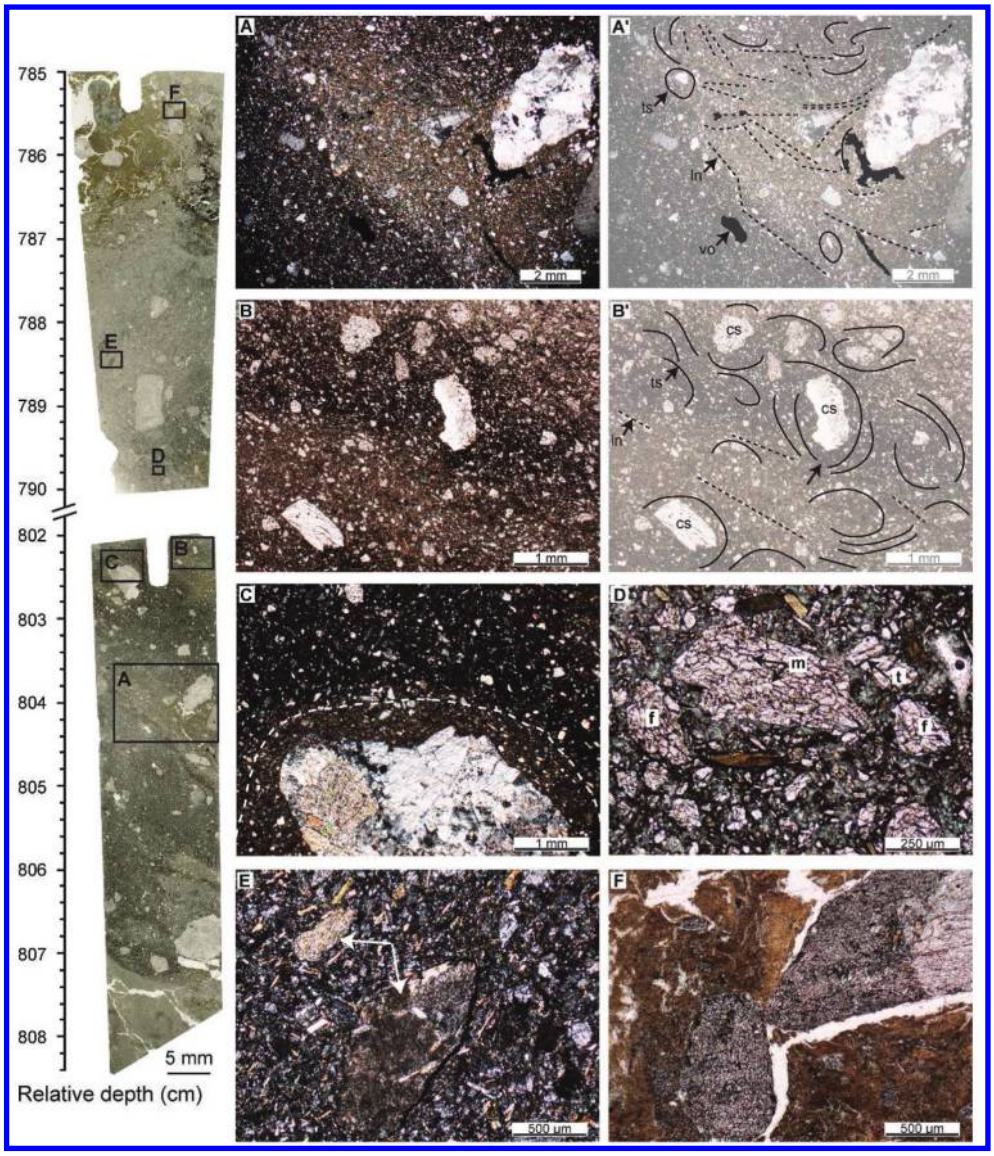

few laminations are also observed. A centimetre-scale sand layer observed around 660 cm depth is characterized by a sharp grain size increase, followed by normal grading indicating a turbidite.

The finely laminated lithofacies is interrupted by a coarse deposit composed of larger particles ranging from 50 μm to 3 mm, with medium rounding and medium to high angularity (Fig. 5E). This heterogeneous bimodal and poorly sorted coarse-grained layer containing rotational structures (Fig. 5E) has folded the underlying laminations and is capped by a normally graded fine sand layer, containing injection structures (Fig. 5G). The shape of the boundary between both layers is irregular and folded (e.g., disharmonic folds) and is characterized by large subangular particles (up to 2 mm) showing flow tails filled by homogeneous fine sand (Fig. 5F). The above rhythmites are strongly deformed (e.g., inverse faults and injection structures) and folded (e.g., antiform folds).

The upper part of Facies IIIa (Fig. 2) is also characterized by finely rhythmically laminated silty clays (Figs. 5H, 5I). Laminations are more horizontal and generally normally graded, mainly from coarse silt to clays. They range in thickness from more than 100 μm to 4–5 mm. The boundary between a fine-grained unit and the overlying coarse-grained unit is often sharp. Single grain lineations within fine-grained units are less common than in the lower part of the facies. No isolated grain >1 mm or load-casting features are any longer observed. Plasmic fabric is absent in this facies.

Facies Ib

Facies Ib has a lower density, as shown by lower grey scale and CT number values, and contains microfossils (Fig. 6). Skeleton grains are distributed homogeneously, range in size from 35 to

Fig. 4. Left panel: Flatbed scan of thin sections of Facies IIIb with corresponding regions of interest (ROI). (A) Comet structure. Plane light. (B) Discontinuous zones of oriented plasma separation forming a masepic plasmic fabric and defining shear zones. Cross-polarized light. (C) Backscattered electron image showing a fluid escape structure (white arrow). Note also the reorientation of small clasts parallel to the surface of a larger one at the bottom left. Their elongated axes are illustrated by black lines. (D) Banded and mottled zone of skeleton grain within fine-grained plasma. Long axis of clasts (black lines) is aligned parallel to bedding (i.e., planar clast fabric). Plane light. (E) Fine to coarse sand zone showing several tails and delimited by alternating silt and clay characterized by high birefringence. The trajectory of a large clast (dropstone) through the sand zone is also visible (white arrow). Plane light. (F) Rotational (galaxy) structure around a well-rounded clast (core stone, cs). Several rounds of oriented clasts are visible and illustrated by white convex lines. Plane light. (G) Pod of homogeneous sandy material (delimited by white line) indicating the nose of the related flow. White dashed lines represent clast reorientation within the flow. Note also the high angle extinction bands within birefringent plasma on the left of the flow nose, corresponding to a kinking plasmic fabric (white arrows). Cross-polarized light. (H) Example of clast halo around a core stone (cs) and delimited by a white circle. Plane light.

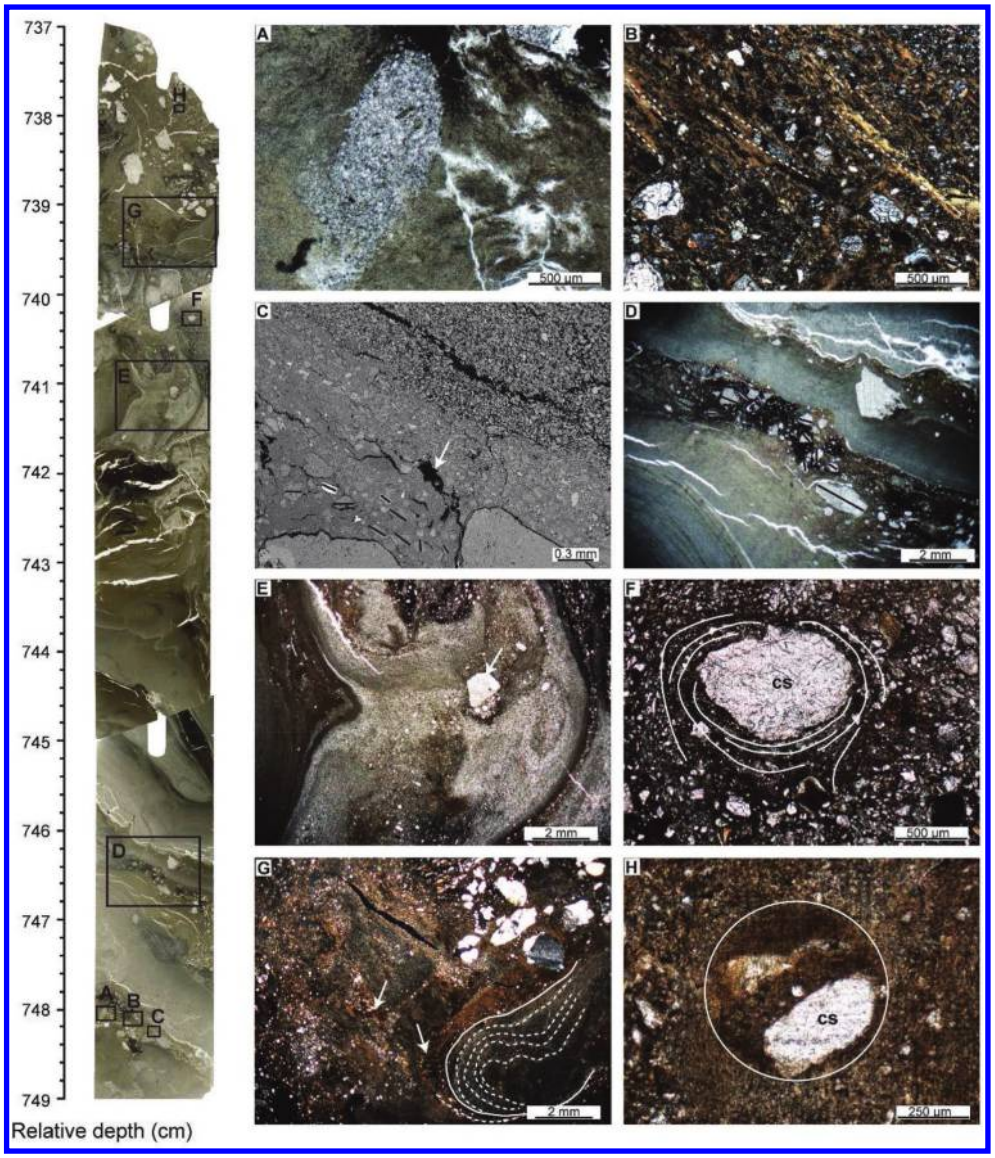

100 µm, and have a medium to high rounding and a low to medium angularity. The plasma consists of fine silt and clay. The coarse-fine related distribution ranges from single- to double-spaced porphyric. Several large clasts (>1 mm) are also observed in places and sometimes concentrated. Coarser clastic deformed and tilted laminations (fine sand or silts) occurred throughout this facies (Fig. 6B). Grains are more angular within the laminations of this facies and the coarse-fine related distribution ranges from close to single-spaced porphyric. The lower contact of the laminations is generally sharp and their grading often normal. No plasmic fabric was observed in this facies, although it clearly displays post-depositional deformations (e.g., wavy folds and convoluted bedding) due to overlying sediments (Fig. 6A). The top of this facies contains injected bands of relatively homogeneous and well-sorted fine to coarse 1–2 mm thick sand layers within finer material (Fig. 6C). Phyllosilicates in this deformed zone have a relatively strong birefringence when viewed under cross-polarized light, which was not observed in the other facies (Fig. 6C).

Facies II

Facies II exhibits very few rotational structures and no crushed grains. No pressure shadows and no obvious plasmic fabric pattern were observed. Contorted sandy layers, recumbent, and slump folds are exclusively observed in this facies (Figs. 7C–7E), and fractured

Fig. 5. Left panel: Flatbed scan of thin sections of Facies IIIa (plane light) with corresponding regions of interest (ROI). (A) Backscattered electron image of a lamination couplet. Note the sharp contact and normal grading of the coarser lamina, and the occurrence of single grain lineation (sgl) of coarser grain in finer laminae. (B) Dropstone in the lower right corner. Note the effect on the laminations below and above. Single grain lines (sgl) are also visible within the millimetre-thick clay layer at the top left. Plane light. (C) Load cast feature observed at the base of a centimetre-thick turbidite resulting locally in strong deformation (up to the destruction) of several lamination couplets below. Note also the well-rounded injection structure of coarse material within silty-clay lamination couplet at the bottom right (white arrow). Plane light. (D) Rhythmites showing normal grading in most beds, while some show multiple laminations. Small-scale load cast features and single grain lineation within darker laminae are also visible. Plane light. (E) Microphotograph and (E′) associated sketch of reoriented skeleton gains (ts, turbate structure; black lines) encircling small gravel particles acting as core stones (cs) and observed in an unsorted and coarser-grained diamictic layer. Plane light. (F) Flow tail filled by homogeneous fine sand behind a subangular clast. Plane light. (G) Load wave structures and well-rounded injection structure within a thick and homogeneous fine sand layer. Plane light. (H) Normal fault (white dashed line) from top left to bottom right in the upper part. Note the absence of load-casting features and dropstones but also the diffuse pattern of the lamination couplets. Cross-polarized light. (I) Some laminae couplets in the upper part showing a similar normal grading, grain size, and sharp lower contact of coarser laminae but also a larger range of thickness variability of the couplets compared to the lower part of the facies. Cross-polarized light.

till pebbles (type III; van der Meer 1993) were also detected (Fig. 7F). The base of this inorganic interval is characterized by an erosional surface as shown on CAT-scan images (Fig. 6) and consists of compact clayish material with injected bands of relatively homogeneous, well-sorted fine to coarse 1–2 mm thick sand layers (Fig. 7A). As for the top of Facies Ib, a relatively strong birefringence of phyllosilicates is observed. Homogeneous fluidized sandy beds are also observed on thin section of the base of Facies II.

Micromorphological study of Facies Ia, corresponding to the surficial organic sediments, is beyond the scope of this paper, as no glacial microstructure or plasmic fabric and post-depositional deformation were observed.

Interpretations and discussion

Facies IV

Facies IV (Table 2) corresponds to a diamicton containing fine skeleton particles that may be oriented parallel to the surface of a large skeleton grain, the core stone. Such grain arrangement (i.e., turbate/rotational/galaxy structure), also observed without a core stone, indicates rotational movement (van der Meer 1993). Similarly, skelsepic and lattisepic plasmic fabrics have developed in response to rotational movement (van der Meer 1993; Menzies 2000), as also suggested by laboratory experiments (Hiemstra and Rijsdijk 2003). The pressure shadow observed in Fig. 3B is also clearly related to this circular arrangement and is generally considered as a good indicator of rotational deformation and shearing (Hanmer and Passchier 1991). Discrete shears (lineations) are also present and reflect brittle deformation, as well as the abundant presence of edge to edge crushed grains. Ductile, brittle, and polyphase (ductile/brittle) deformations thus occur throughout the deposit, strongly suggesting that high stress conditions contributed to its formation, especially with the fracture of individual quartz grains. The presence of crushed grains in glacial diamictons has only been reported and described from basal till (Hiemstra and van der Meer 1997; Carr 1999; Menzies and Zaniewski 2003), and their presence or absence may thus be used as a diagnostic criterion to determine the diamicton type (Larsen et al. 2007). Furthermore, the grain shape may indicate edge abrasion currently observed in subglacial settings (e.g., Carr et al. 2006). All the microstructures and microfabrics observed in Facies IV are commonly found in subglacial till (van der Meer 1993) where large tangential stresses have been applied. On the other hand, sediment flow deposits share many of them (Lachniet et al. 2001). Facies IV was likely formed at the base of the ice sheet outside the crater and was entrained over the study site during the glaciation, before flowing in a subglacial lake environment during the last deglaciation. This interpretation is consistent with the core stratigraphy and the evidence of external input of glacially derived materials in the crater lake basin, as highlighted by the presence of U-rich material and by infra-red stimulated luminescence estimates (Guyard et al. 2011). In addition, pollen analysis in Facies IV and Facies III revealed a relatively high abundance of *Picea* and *Pinus* sp. grains (Girard-Cloutier, 2010). The pollen of these two species are found in the nearby and exceptionally pollen-rich tills (Richard et al. 1991; Fréchette et al. 1996) and reflect their remobilization and incorporation from former interglacial/interstadial periods at the base of the ice sheet and their deposition in the lake during later deglaciation (Guyard et al. 2011). A few diatoms were also observed around 820 cm and at the top of the facies (Black et al. 2010) and mainly correspond to *Aulacoseira* spp., a diatom genus known to be able to grow under a thin ice cover (Bondarenko et al. 2006). These diatoms were unlikely preserved and remobilized from the same till surrounding the crater, as neither diatoms nor other lacustrine sediment vestiges were reported in the regional till (e.g., Fréchette et al. 1996), but rather they reflect the environmental conditions that occurred during the last deglaciation under permanent thin ice cover conditions. This very dense diamicton was thus released by the passive ablation of debris-rich basal glacier ice (i.e., subglacial meltout in a 250 m deep subaquatic environment) that marked the end of subglacial conditions. The deposit presents structures inherited from the source material and structures likely formed during sediment flowage and deposition (Lachniet et al. 2001). The range of microstructures observed in Facies IV (Table 2) probably does not reflect the full complexity of the diamicton genesis, as some original strain structures may also have been overprinted during flowage.

Facies IIIb

Facies IIIb (Table 2) represents a highly disturbed and heterogeneous interval displaying numerous microstructures indicative of porewater-influenced and (or) controlled deformations, including fluid escape structures, clast haloes, and the presence of beds or zones of liquified sands and silts forming lubricated detachments (Fig. 4). Because variations in water content influence the style and apparent intensity of deformation recorded (Phillips et al. 2007), they testify to the presence of water during deposition. The change in porewater content between Facies IV and Facies IIIb likely resulted in liquefaction (Allen 1977) of Facies IIIb and overprinted some of the pre-existing deformation microstructures by homogenizing the sediments (e.g., Figs. 4D, 4E). Based on core stratigraphy and multiproxy analyses, Guyard et al. (2011) suggested that this deposit resulted from a glacigenic sediment gravity flow. The assemblage of the glacial microstructures (Table 2) provides additional evidence and information about the sediment flowage and deposition. For instance, some load-casting features, as well as rare turbate structures, indicate rotational movement and relatively high strain levels. The clay coating surrounding the whole sand and pebble grains, reflecting continuous rotational movement of the grains in a turbulent lacustrine environment (Kilfeather et al. 2010), also indicate that the gravity flow had a long run-out distance from the lake surface. Moreover, banded and mottled plasma have been reported when mixing of different sediment

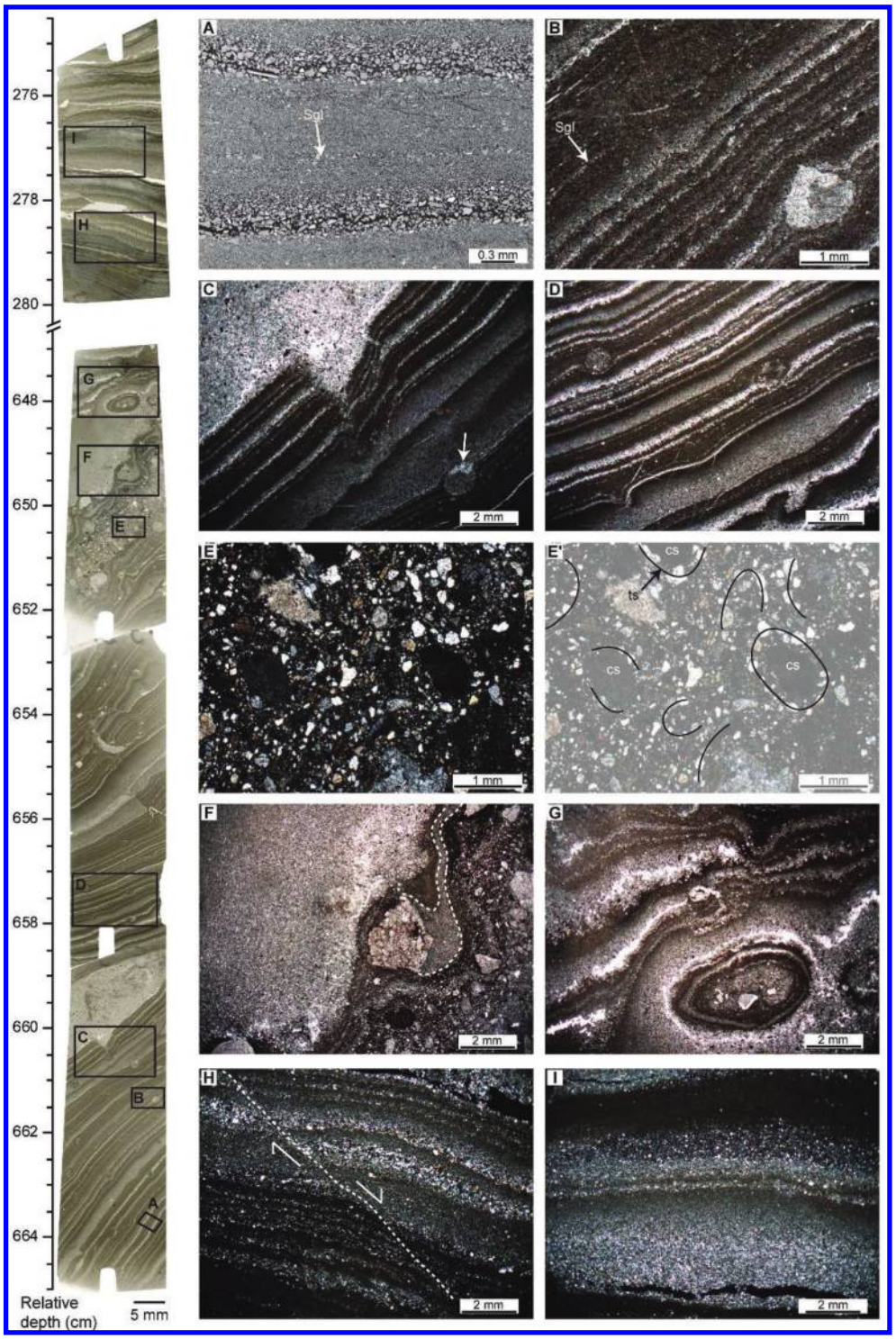

facies occurred without completely homogenizing the sediment (van der Meer and Menzies 2011). Kinking plasmic fabric also reflects strong shearing in a compressional regime (Menzies and Maltman 1992; Bordonau and van der Meer 1994). Facies IIIb could thus result from the efflux plume and the associated suspension sedimentation produced during the final southwestward retreat of the ice sheet margin (Bouchard and Marcotte 1986) from the catchment area (see below). Indeed, the processes of transport and deposition occurring within this depositional environment would also explain the complex and mixing sedimentary information derived from companion studies (Black et al. 2012; Girard-Cloutier 2010; Guyard et al. 2011; Luoto et al. 2013). According to these studies, the core stratigraphy, the organic carbon content and composition, the abundance of diatoms characteristic of open water, the dominance of the Cyperaceae pollen, and the zoological remains (e.g., Cladocera) indicate a depositional environment under temporarily ice-free conditions in a proglacial context prior to the final deglaciation.

Facies IIIa

Finely and continuously laminated meltout silts are then observed in the overlying Facies IIIa and described as rhythmites

Fig. 6. Left panel: CAT-scan (CT) image of Facies Ib with underlying finely laminated meltout sediments (top of previous Facies IIIa; Figs. 5I, 5J) and the upper erosive contact and contorted layers within Facies II (Fig. 7). Note the sharp increase of CT numbers (CTn) at the base of Facies II, reflecting an abrupt change in bulk density. The right panels show Facies Ib micromorphology. (A) Backscattered electron image illustrating postdepositional deformation of organic sediments (darker grey on CAT-scan images). Diatoms are visible. (B) Backscattered electron image showing normally graded and tilted coarse silt laminae, also recorded by higher CTn values and lighter grey scale. Note the presence of microfossils (diatoms). (C) Injected homogeneous, fine sand channels at the top of postglacial sediments. Note the high birefringence of the clays near the channels. Cross-polarized light.

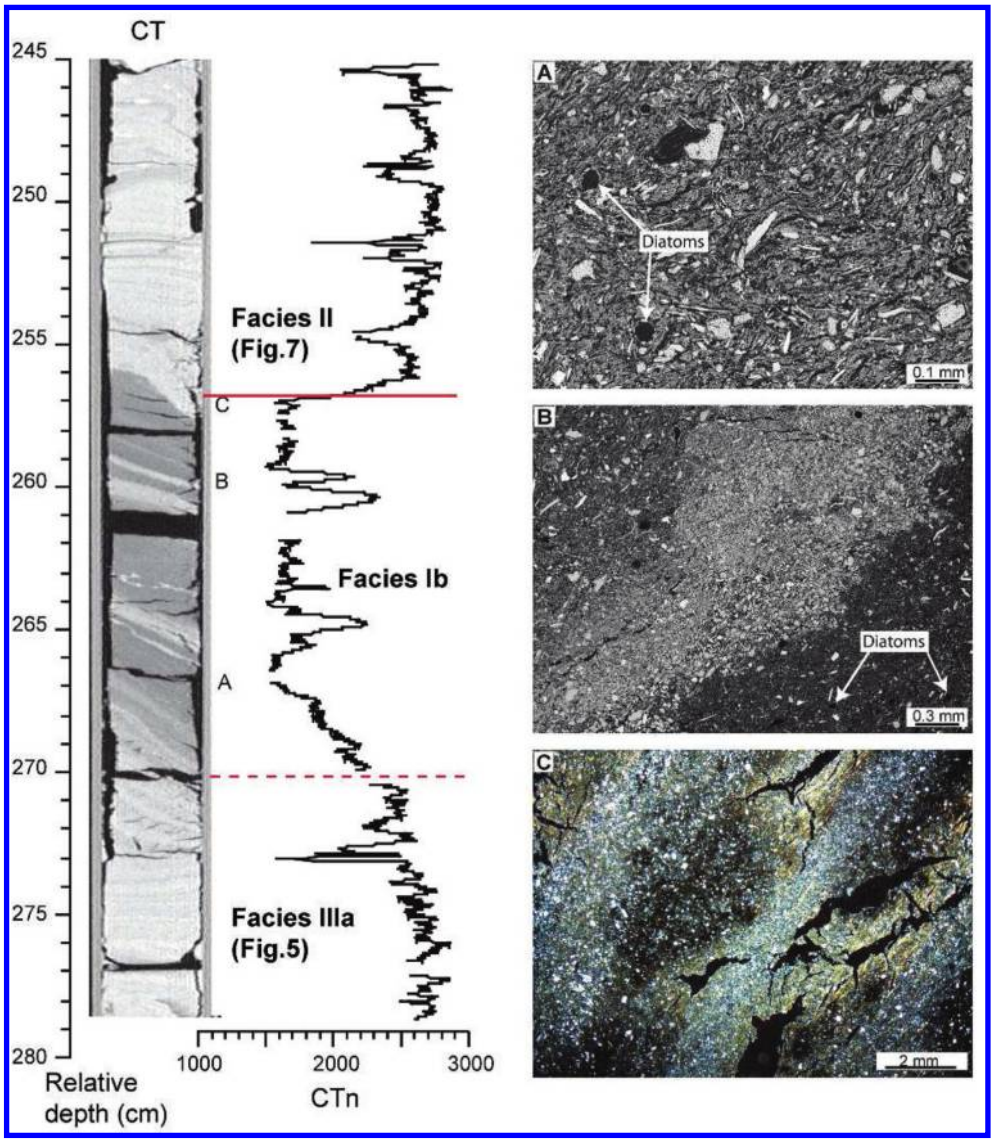

(Fig. 5). Deposition of rhythmites and clays occurred in an unstable environment (Jørgensen 1981), characterized here by synsedimentary faulting, folding, water escape, and load casting, reflecting rapid deposition and high sedimentation rates. If the causal factors for the periodicity of the rhythmites and the duration of lamination couplet deposition cannot be specified here, the change in the associated sedimentary inputs into the basin is likely related to the presence of ice. Occasional dropstones and load-casting features disturb the (originally) regular laminations (Figs. 5B–5D) and suggest an ice-marginal lacustrine environment even though some of the sand dropstones could also have resulted from niveo-aeolian processes (e.g., Lewis et al. 2002) and (or) from the erosion of the crater rim. In such environments, the presence of floating ice blocks is not uncommon even if the ice front is far away (Ashley 1995). As meltwater inlets from the glacier were probably absent at that time, especially because of the high elevation of the crater (Fig. 1), these glacigenic meltwater silts may originate from drifting icebergs or floating ice blocks. This is supported by AMS ^{14}C dates in Facies IIIa that also reflect glacially derived meltout material (Guyard et al. 2011). The regular grading of most of the coarser laminae from Facies IIIa and their sharp contact suggests that they were mainly deposited by settling from sediment density underflows, a common process in freshwater ice-marginal lakes (Sturm and Matter 1978; Moscariello 1996). Such laminae vary in thickness and (or) grain size depending on the amount of meltwater and sediment supply. The finer and clayey part of the laminations would result from suspension settling. In some instances, overflow may also form by meltwater but only if a thermocline is developed (Ashley 1995). Single grain laminations within fine-grained units (Figs. 5A, 5B) may reflect the rain out of coarser grains resulting from such overflows (van der Meer and Warren 1997) and thus suggest the possible and occasional presence of a thermocline depending on ice cover conditions. Coarser, thicker, and ungraded glacigenic deposits are also

Fig. 7. Left panel: Flatbed scan of thin sections of Facies II with corresponding regions of interest (ROI). (A) Clastic injections at the base of the mass wasting deposit. Note the high birefringence of the clays near the channels associated with the injection. Cross-polarized light. (B) Deformed sandy laminations caused by upward-escaping fluids in the sediments. A coarse sandy body in the upper right corner has resulted in complete disturbance of bedding. Plane light. (C) Contorted sandy layer, folds, and multiple diamicton domains. Plane light. (D) Contorted sandy layers and folds within coarse grain diamicton. Plane light. (E) Slump folds. Plane light. (F) Clay-fractured pebbles (white arrow). Cross-polarized light.

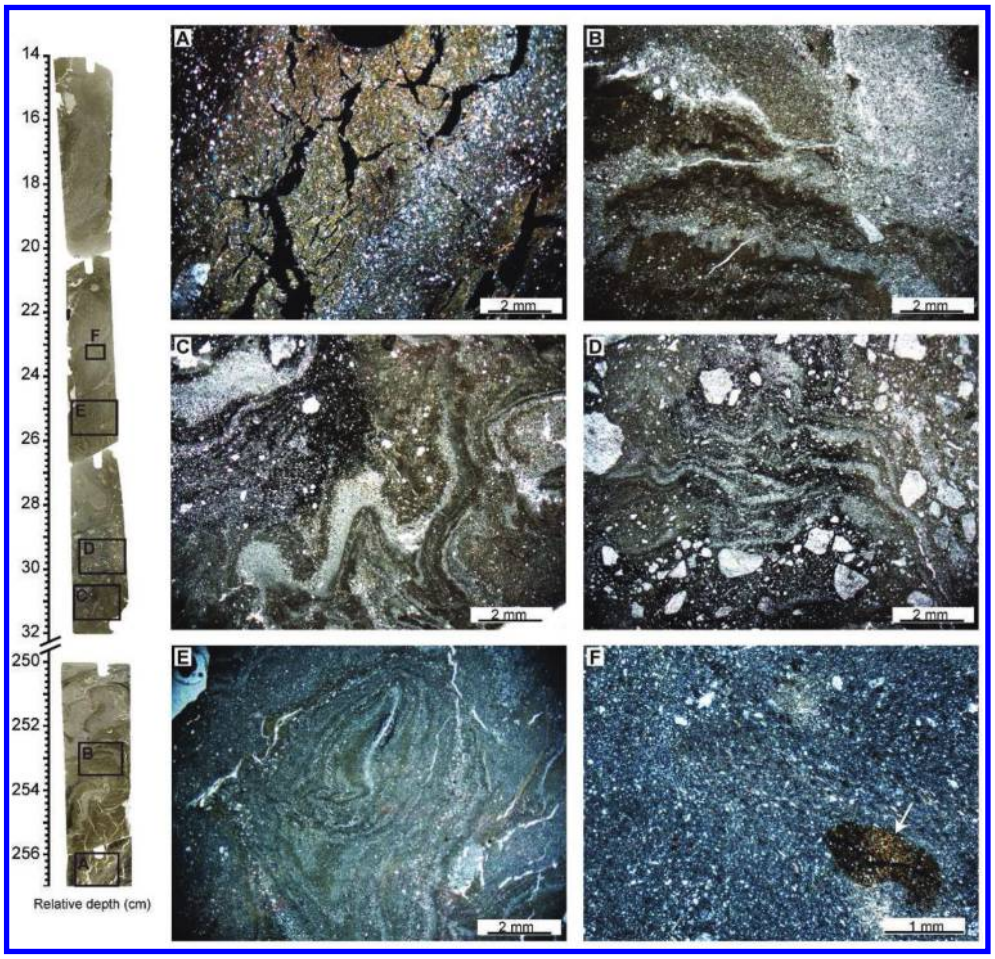

detected throughout Facies IIIa, contain rotational (Fig. 5E), flow tail (Fig. 5F), and injection (Fig. 5G) structures, and result in deformation of the underlying laminae (microfolds and microfaults). This indicates a rapid deposition originating from iceberg rafting and may reflect the absence of the development of shorefast lake ice, allowing them to drift and release more basal material, as previously reported in Greenland fjords (Ó Cofaigh and Dowdeswell 2001). This is consistent with ice cover period fluctuations detected throughout the lithofacies inferred from geochemical proxies (e.g., $\delta^{13}C$ and Fe/Ti ratio) and diatom assemblages (Guyard et al. 2011; Black et al. 2010). If the ice margin proximity had influenced the creation of the laminations, then a decrease of the grain size should be expected in the top of the sequence, as the coarser particles would be deposited in the more proximal basins. The constant grain size and sharp contact of the laminae observed throughout Facies IIIa rule out this interpretation and further confirm that the meltwater originated from the drifting glacial ice blocks and thus the isolation of the basin from the disintegrating ice sheet in the last stages of deglaciation. Nevertheless, the upper laminations are not affected by load casting and no dropstones were detected (Figs. 5H, 5I), indicating a more stable and less energetic depositional environment, implying weaker glacially derived clastic inputs. The more diffuse pattern of laminae and their horizontal orientation may also reflect thinner ice and lower sedimentation rates. Pollen data from this interval indicate the development of herbaceous tundra vegetation associated with a warming period, also suggesting a decrease of lake ice cover (Girard-Cloutier 2010).

Facies Ib

Facies Ib (Table 2) is more organic, contains smaller detritic grains, and the absence of glacial microstructures and rhythmites indicates a stable and less energetic depositional environment associated with the final disappearance of the remnant drifting ice blocks. Facies Ib corresponds to the onset of the postglacial period ca. 6850 cal years BP (Guyard et al. 2011), the inception of lacustrine productivity (Black et al. 2012; Luoto et al. 2013), and the development of shrub tundra in the surrounding area (Girard-Cloutier 2010). The occasional presence of coarser, graded and tilted laminae (Fig. 6A) may reflect ice cover periods or distal turbidites, such as those observed in similar settings (e.g., El'Gygytgyn Crater Lake, Sauerbrey et al. 2013). This interval is also affected by post-depositional deformation (Figs. 6A, 6B) and sand injection (Fig. 6C) related to the above MWD (Facies II).

Facies II

Microstructures, such as rotational structures and multiple lineations are rare in Facies II (Table 2), indicating a relatively low overburden pressure typical of mass movement sediments (Menzies and Whiteman 2009). Velocity of motion and especially porewater

Table 2. Summary of microfabrics and microstructures within the plasma and S-matrix observed in each lithofacies.

Microstructures			Facies IV	IIIb	IIIa	Ib	II
Plasmic fabric	Masepic			•			
	"Banded" plasma			•			
	"Kinking" plasmic fabric			•			
	Lattisepic		•				
	Skelsepic		•				
S-matrix	Ductile	Strain caps and shadows	•				
		Fold		•	•	••	•••
		Necking	••	•			
		Rotational structures	••	•	•		•
		Bounding	•				
	Brittle	Faults			•		
		Discrete shear lines and lineations	••	•		•	•
		Shear zone	••	•			
		Reverse fault			•		
		Crushed grains	••				
	Polyphase	Multiple diamicton domains	••				•
		Comet structures		•			
		Intraclasts	•				•
	Pore water influenced or induced	Water escape structures		••	•		•
		Silt caps		•			
		Silt and clay coating	•	••			

Note: The presence of a single dot identifies the presence of a particular feature, while two or three dots indicate much more developed and common structures, according to Carr (1999).

content influences the nature of sediment mass movements (Lachniet et al. 1999). The rarely developed porewater structures associated with porewater dissipation, the absence of grain crushing events, the short distance lineations, and the much higher ductile deformations attest of a subaqueous wet mass movement (Lachniet et al. 1999; Menzies and Whiteman 2009). The contorted sandy layers and internal deformations suggest a rotational slide (i.e., slump) (Mulder and Cochonat 1996; Guyard et al. 2007*b*) and the slump folds (i.e., intraformational folds produced by deformation of soft sediments) are observed exclusively in Facies II. Microstructure analysis at the base of the MWD, characterized by a chaotic facies on acoustic profiles (Guyard et al. 2011), reveals intense soft-sediment deformation indicative of fluidization and high stress level associated with the sand injection (which is likely part of the mass movement), as indicated by the high clay birefringence that was not observed in the other facies. Moreover, many of the coarse sandy bodies observed on thin sections appear to have orientation or even tails, suggesting derivation from previously more coherent bodies, i.e., formerly in place sediment. The presence of till pebbles points to a remobilization of former glacigenic deposits, as also suggested by stratigraphic data (Guyard et al. 2011). According to these authors, the slump may have been triggered by slope instabilities or an increased seismic activity associated with rapid glacio-isostatic rebound, as well as by rapid lake discharge events following the last deglaciation (Desiage et al. 2014; Guyard et al. 2011).

Conclusions

A large set of microstructures from glacial sediments and related to the S-matrix are recognized in Pingualuit Crater Lake sediments and reflect ductile (e.g., folds, turbate and galaxy structures, strain caps and shadows), brittle (e.g., faults, shear, lineation, crushed grains), polyphase (e.g., "comet" structure, intraclasts, multiple diamicton domains), or porewater-influenced (e.g., water escape structures, silt and clay coating) deformations in a complex subglacial lake environment in the context of the last deglaciation. The assemblage of different microstructure types observed (Table 2) provided valuable additional insights into the sedimentary dynamics and the depositional subenvironments of deformed glacigenic and postglacial lithofacies within this unusual environment. The depositional mechanisms and processes described from the Pingualuit Crater Lake sediments (subglacial meltout, gravity flow, underflows, suspension settling) are consistent with several sedimentary processes described in other former but much larger subglacial lakes under the LIS, such as Subglacial Lake McGregor (Munro-Stasiuk 2003) and Great Slave Lake (Christoffersen et al. 2008), as well as with conceptual models of sedimentation in subglacial lakes (Bentley et al. 2011; Livingstone et al. 2012). Sediments from the last deglaciation contain several microfacies assemblages pointing to a mixture of proglacial and ice-marginal environments, with a general evolution from a subglacial lake environment to an ice-marginal environment that precedes the postglacial conditions. A slump composed of reworked glacigenic deposits in postglacial sediments is easily distinguished from other intervals from its microstructures, suggesting overprinting of preexisting deformation microstructures during the flow and deposition of the slump. The latter has deformed the underlying postglacial organic sediments and may have perturbed the associated climatic and (or) environmental record. A good understanding of sedimentary environments and depositional processes is thus essential to better read into paleoenvironmental proxies contained within these complex subglacial lake sediments.

Acknowledgements

This research received financial support from the Canadian Foundation for Climate and Atmospheric Sciences (CFCAS), the Natural Sciences and Engineering Research Council of Canada (NSERC), and the International Association of Sedimentologists (IAS). The authors acknowledge Richard Niedereiter (UWITEC), Veli-Pekka Salonen (University of Helsinki), the Pingualuit National Park employees, and the inhabitants of the hamlet of Kangiqsujuaq for their help and support during the challenging field expeditions. Thanks are due to Jacques Labrie (ISMER), Frédéric Bouchard (INRS-ETE), and Guillaume Jouve (INRS-ETE) for their help in the laboratory. The authors also acknowledge Flavio Anselmetti (University of Bern), John Menzies (Brock University), and Nick Eyles (University of Toronto) for their comments on an earlier draft of this paper, as well as two anonymous reviewers and the associate editor for their constructive reviews.

References

Allen, J.R.L. 1977. The possible mechanics of convolute lamination in graded sand beds. Journal of the Geological Society (London), **134**: 19–31. doi:10.1144/gsjgs.134.1.0019.

Ashley, G.M. 1995. Glaciolacustrine environments. *In* Glacial Environments, vol. 1: Modern glacial environments, processes dynamics and sediments. *Edited by* J. Menzies. Butterworth Heinemann, Oxford. pp. 417–444.

Bell, R.E., Studinger, M., Shuman, C.A., Fahnestock, M.A., and Joughin, I. 2007. Large subglacial lakes in East Antarctica at the onset of fast-flowing ice streams. Nature **445**: 904–907. doi:10.1038/nature05554.

Bentley, M.J., Christoffersen, P., Hodgson, D.A., Smith, A.M., Tulaczyk, S., and Le Brocq, A.M. 2011. Subglacial lake sedimentary processes: potential archives of ice sheet evolution, past environmental change and the presence of life. *In* Antarctic subglacial aquatic environments. *Edited by* M.J. Siegert and C. Kennicutt. American Geophysical Union, Washington D.C. doi:10.1002/9781118670354.ch6.

Black, J.L., Hausmann, S., Pienitz, R., St-Onge, G., Guyard, H., Salonen, V.-P., et al. 2010. Reconstruction of paleoenvironmental changes from Pingualuit Crater Lake sediments during glacialinterglacial cycles MIS 1 to MIS 8: A Long-term terrestrial record from the Canadian Arctic. European Geophysical Union, Vienna, Austria. p. 9671.

Black, J.L., Edlund, M.B., Hausmann, S., and Pienitz, R. 2012. Small freshwater thalassiosiroid diatoms from Pleistocene sediments of Pingualuit Crater Lake, northern Québec (Canada), including description of *Cyclotella pingualuitii* sp. nov. Diatom Research, **27**(1): 53–63. doi:10.1080/0269249X.2012.654825.

Boespflug, X., Long, B.F.N., and Occhietti, S. 1995. CAT-scan in marine stratigraphy: a quantitative approach. Marine Geology, **122**: 281–301. doi:10.1016/0025-3227(94)00129-9.

Bondarenko, N.A., Timoshkin, O.A., Röpstorf, P., and Melnik, N.G. 2006. The under-ice and bottom periods in the life cycle of *Aulacoseira baicalensis* (K. Meyer) Simonsen, a principal Lake Baikal alga. Hydrobiologia, **568**(Suppl 1): 107–109. doi:10.1007/s10750-006-0325-7.

Bordonau, J., and van de Meer, J.J.M. 1994. An example of a kinking microfabric in upper-Pleistocene glaciolacustrine deposits from Llavorssi (Central Southern Pyrenées, Spain). Netherlands Journal of Geosciences (Geologie en Mijnbouw), **73**(1): 23–30.

Bouchard, M.A. 1989. L'histoire naturelle du Cratère du Nouveau-Québec. Collection Environnement et Géologie, vol. 7. Université de Montréal. 420 p.

Bouchard, M.A., and Marcotte, C. 1986. Regional glacial dispersal patterns in Ungava, Nouveau-Québec. Geological Survey of Canada, paper 86-1B: 295–304.

Brewer, R. 1976. Fabric and mineral analyses of soils. Krieger, Huntington, NY, 482 p.

Carr, S.J. 1999. The micromorphology of last glacial maximum sediments in the southern North Sea. Catena, **35**: 123–145. doi:10.1016/S0341-8162(98)00097-6.

Carr, S.J., Holmes, R., van der Meer, J.J.M., and Rose, J. 2006. The last glacial maximum in the North Sea Basin: micromorphological evidence of extensive glaciations. Journal of Quaternary Science, **21**: 131–153. doi:10.1002/jqs.950.

Christoffersen, P., Tulaczyk, S., Wattrus, N.J., Peterson, J., Quintana-Krupinski, N., Clark, C., and Sjunneskog, C. 2008. Large subglacial lake beneath the Laurentide ice sheet inferred from sedimentary sequences. Geology, **36**: 563–568. doi:10.1130/G24628A.1.

Daigneault, R.-A. 1997. Géologie des formations en surface, région du cap de Nouvelle-France, du cratère du Nouveau-Québec et de Kangiqsujuaq, Québec-Territoires du Nord-Ouest. Commission géologique du Canada, Carte 1863A. doi:10.4095/208999.

Daigneault, R., and Bouchard, M.A. 2004. Les écoulements et le transport glaciaires dans la partie septentrionale du Nunavik (Québec). Canadian Journal of Earth Sciences, **41**(8): 919–938. doi:10.1139/e04-048.

Desiage, P.-A. 2014. Évolution tardi-quaternaire et morpho-stratigraphie des sédiments du cratère des Pingualuit : variation du niveau du lac, origine des mouvements de masse et influence de la glaciation wisconsinienne. M.Sc. thesis, Université du Québec à Rimouski. 56 p.

Dyke, A.S., and Prest, V.K. 1987. Late Wisconsinan and Holocene history of the Laurentide ice sheet. Géographie Physique et Quaternaire, **41**: 237–263. doi:10.7202/032681ar.

Evatt, G.W., Fowler, A.C., Clark, C.D., and Hulton, N.R.J. 2006. Subglacial floods beneath ice sheets. Philosophical Transactions of the Royal Society A: Mathematical, Physical and Engineering Sciences, **364**: 1769–1794. doi:10.1098/rsta.2006.1798.

Fortin, D., Francus, P., Gebhardt, A.C., Hahn, A., Kliem, P., Lisé-Pronovost, A., et al., PASADO Science Team. 2013. Destructive and non-destructive density determination: method comparison and evaluation from the Laguna Potrok Aike sedimentary record. Quaternary Science Reviews, **71**: 147–153. doi:10.1016/j.quascirev.2012.08.024.

Francus, P., and Cosby, C.A. . 2001. Sub-sampling unconsolidated sediments: a solution for the preparation of undisturbed thin-sections from clay-rich sediments. Journal of Paleolimnology, **26**(3): 323–326. doi:10.1023/A:1017572602692.

Fréchette, B., Bouchard, M.A., and Richard, P.J.H. 1996. Le till pollinifère de la péninsule du Nunavik, Québec septentrional. Géographie physique et Quaternaire, **50**(3): 331–340.

Gantner, N., Veillette, J., Michaud, W.K., Bajno, R., Muir, D., Vincent, W.F., et al. 2011. Physical and biological factors affecting mercury and perfluorinated contaminants in Arctic char (*Salvelinus alpinus*) of Pingualuit Crater Lake (Nunavik, Canada). Arctic, **65**(2): 195–206. doi:10.14430/arctic4200.

Girard-Cloutier, A-M. 2010. Reconstitution paléobotanique et paléoclimatique en Ungava: Analyse pollinique des sédiments du Cratère des Pingualuit. M.Sc. Thesis, Département de géographie, Université Laval. 68 p.

Grieve, R.A.F., Bottomley, R.B., Bouchard, M.A., Robertson, P.B., Orth, C.J., and Attrep, M. 1991. Impact melt rocks from New Quebec Crater, Quebec, Canada. Meteoritics, **26**: 31–39. doi:10.1111/j.1945-5100.1991.tb01012.x.

Guyard, H., Chapron, E., St-Onge, G., Anselmetti, F.S., Arnaud, F., Magand, O., et al. 2007*a*. High-altitude varve records of abrupt environmental changes and mining activity over the last 4000 years in the western French Alps (Lake Bramant, Grandes Rousses Massif). Quaternary Science Reviews, **26**: 2644–2660. doi:10.1016/j.quascirev.2007.07.007.

Guyard, H., St-Onge, G., Chapron, E., Anselmetti, F. and Francus, P. 2007*b*. The AD 1881 earthquake-triggered a slump and late Holocene flood-induced turbidites from proglacial Lake Bramant, Western French Alps. *In* Submarine mass movements and their consequences. Vol. 27. *Edited by* V. Lykousis, D. Sakellariou and J. Locat. Kluwer-Springer. pp. 279–286. doi:10.1007/978-1-4020-6512-5_29.

Guyard, H., St-Onge, G., Pienitz, R., Francus, P., Zolitschka, B., Clarke, G.K.C., et al. 2011. New insights into Late Pleistocene glacial and postglacial history of northernmost Ungava (Canada) from Pingualuit Crater Lake sediments. Quaternary Science Reviews, **30**: 3892–3907. doi:10.1016/j.quascirev.2011.10.002.

Hanmer, S., and Passchier, C. 1991. Shear-sense indicators: a review. Geological Survey of Canada, paper 90-17. 72 p.

Hiemstra, J.F., and Rijsdijk, K.F. 2003. Observing artificially induced strain: implications for subglacial deformation. Journal of Quaternary Science, **18**: 373–383. doi:10.1002/jqs.769.

Hiemstra, J.F., and van der Meer, J.J.M. 1997. Pore-water controlled grain fracturing as an indicator for subglacial shearing in tills. Journal of Glaciology, **43**(145): 446–454.

Hodgson, D.A., Roberts, S.J., Bentley, M.J., Carmichael, E.L., Smith, J.A., Verleyen, E., et al. 2009. Exploring former subglacial Hodgson Lake, Antarctica. Paper II: Palaeolimnology. Quaternary Science Reviews, **28**(23–24): 2310–2325. doi:10.1016/j.quascirev.2009.04.014.

Jørgensen, N.B. 1981. Turbidites and associated resedimented deposits from a tilted glacio-deltaic sequence, Denmark. Danmarks geologiske undersøgelse, Årbog: 47–92.

Kilfeather, A.A., Ó Cofaigh, C., Dowdeswell, J.A., van der Meer, J.J.M., and Evans, D.J.A. 2010. Micromorphological characteristics of glacimarine sediments: implications for distinguishing genetic processes of massive diamicts. Geo-Marine Letters, **30**(2): 77–97. doi:10.1007/s00367-009-0160-8.

Krumbein, W.C. 1941. Measurement and geological significance of shape and roundness of sedimentary particles. Journal of Sedimentary Petrology, **11**: 64–72. doi:10.1306/D42690F3-2B26-11D7-8648000102C1865D.

Lachniet, M.S., Larson, G.J., Strasser, J.C., Lawson, D.E., Evenson, E.B., and Alley, R.B. 1999. Microstructures of glacigenic sediment-flow deposits, Matanuska Glacier, Alaska. *In* Glacial processes past and present. *Edited by* D.M. Mickelson and J.W. Attig. Geological Society of America, Boulder, Colorado. Special Paper 337. pp. 45–57.

Lachniet, M.S., Larson, G.J., Lawson, D.E., Evenson, E.B., and Alley, R.B. 2001. Microstructures of sediment flow deposits and subglacial sediments: a comparison. Boreas, **30**: 254–262. doi:10.1080/030094801750424166.

Lamoureux, S.F. 1994. Embedding unfrozen lake sediments for thin section preparation. Journal of Paleolimnology, **10**: 141–146. doi:10.1007/BF00682510.

Larsen, N.K., Piotrowski, J.A., and Menzies, J. 2007. Microstructural evidence of low-strain, time-transgressive subglacial deformation. Journal of Quaternary Science, **22**: 593–608. doi:10.1002/jqs.1085.

Lauriol, B., and Gray, J.T. 1987. The decay and disappearance of the late Wisconsin ice sheet in the Ungava Peninsula, northern Québec, Canada. Arctic and Alpine Research, **19**: 109–126. doi:10.2307/1551245.

Ledoux, G., Lajeunesse, P., Philibert, G., Sinkunas, B., Guyard, H., St-Onge, G., et al. 2011. Morpho-stratigraphy of Pingualuit Crater Lake, Ungava Peninsula, Nunavik. 41th Arctic Workshop, Montreal, Canada. p. 179.

Lewis, T., Gilbert, R., and Lamoureux, S.F. 2002. Spatial and temporal changes in sedimentary processes at proglacial Bear Lake, Devon Island, Nunavut, Canada. Arctic, Antarctic, and Alpine Research, **34**(2): 119–129. doi:10.2307/1552463.

Livingstone, S.J., Clark, C.D., Piotrowski, J.A., Tranter, M., Bentley, M.J., Hodson, A., et al. 2012. Theoretical framework and diagnostic criteria for the identification of palaeo-subglacial lakes. Quaternary Science Reviews, **53**: 88–110. doi:10.1016/j.quascirev.2012.08.010.

Luoto, T.P., Salonen, V., Larocque-Tobler, I., Pienitz, R., Hausmann, S., Guyard, H., and St-Onge, G. 2013. Pro- and postglacial invertebrate communities of the Pingualuit Crater Lake, Nunavik (Canada), and their paleoenvironmental implications. Freshwater Science, **32**(3): 951–963. doi:10.1899/12-178.1.

Menzies, J. 1998. Microstructures within subglacial diamictons. *In* Relief and deposits of present-day and pleistocene glaciations of the northern hemisphere — selected problems. *Edited by* A. Kostrzewski and A. Michiewicz. University Press, Geography Series, Poznan **58**. pp. 210–216.

Menzies, J. 2000. Micromorphological analyses of microfabrics and microstructures indicative of deformation processes in glacial sediments. *In* Deformation of glacial materials. *Edited by* A.J. Maltman, B. Hubbard and

M.J. Hambrey. Geological Society of London. Special Publication 176. pp. 245–257. doi:10.1144/GSL.SP.2000.176.01.19.
Menzies, J., and Maltman, A.J. 1992. Microstructures in diamictons — evidence of subglacial bed conditions. Geomorphology, **6**: 27–40. doi:10.1016/0169-555X(92)90045-P.
Menzies, J., and Whiteman, C.A. 2009. A comparative analysis of microstructures from Late Jurassic diamictic units, near Helmsdale, northeast Scotland and a Pleistocene diamicton from near Milton, southern Ontario, Canada — a differential diagnostic method of sediment typing using micromorphology. Netherlands Journal of Geosciences (Geologie en Mijnbouw), **88**(1): 75–94.
Menzies, J., and Zaniewski, K. 2003. Microstructures within a modern debris flow deposit derived from Quaternary glacial diamicton — a comparative micromorphological study. Sedimentary Geology, **157**: 31–48. doi:10.1016/S0037-0738(02)00193-8.
Moscariello, A. 1996. Quaternary geology of the Geneva Bay: sedimentary record, palaeoclimatic and paleoenvironmental reconstruction since the Last Glacial Cycle. Ph.D. Thesis, Terre et Environnement, University of Geneva. 230 p.
Mulder, T., and Cochonat, P. 1996. Classification of offshore mass movements. Journal of Sedimentary Research, **66**(1): 43–57. doi:10.1306/D42682AC-2B26-11D7-8648000102C1865D.
Munro-Stasiuk, M.J. 2003. Subglacial Lake McGregor, south-central Alberta, Canada. Sedimentary Geology, **160**: 325–350. doi:10.1016/S0037-0738(03)00090-3.
Ó Cofaigh, C., and Dowdeswell, J.A. 2001. Laminated sediments in glacimarine environments: diagnostic criteria for their interpretation. Quaternary Science Reviews, **20**: 1411–1436. doi:10.1016/S0277-3791(00)00177-3.
Phillips, E., Merritt, J., Auton, C.C., and Golledge, N. 2007. Microstructures in subglacial and proglacial sediments: understanding faults, folds and fabrics, and the influence of water on the style of deformation. Quaternary Science Reviews, **26**: 1499–1528. doi:10.1016/j.quascirev.2007.03.007.
Pienitz, R., Melles, M., and Zolitschka, B. 2009. Results of recent sediment drilling activities in deep crater lakes. PAGES News, **17**(3): 117–118.
Rawling, G.C., and Goodwin, L.B. 2003. Cataclasis and particulate flow in faulted, poorly lithified sediments. Journal of Structural Geology, **25**: 317–331. doi:10.1016/S0191-8141(02)00041-X.
Rémillard, A.M., Hétu, B., Bernatchez, P., and Bertran, P. 2013. The drift des Demoiselles on the Magdalen Islands (Québec, Canada): sedimentological and micromorphological evidence of a Late Wisconsinan glacial diamict. Canadian Journal of Earth Sciences, **50**(5): 545–563. doi:10.1139/cjes-2011-0115.
Richard, P.J.H., Bouchard, M.A., and Gangloff, P. 1991. The significance of pollen-rich inorganic lake sediments in the Cratère du Nouveau-Québec area, Ungava, Canada. Boreas, **20**(2): 135–149. doi:10.1111/j.1502-3885.1991.tb00302.x.
Sauerbrey, M.A., Juschus, O., Gebhardt, A.C., Wennrich, V., Nowaczyk, N.R., and Melles, M. 2013. Mass movement deposits in the 3.6 Ma sediment record of Lake El'gygytgyn, Far East Russian Arctic. Climate of the Past, **9**(4): 1949–1967. doi:10.5194/cp-9-1949-2013.
Seret, G. 1993. Microstructures in thin sections of several kinds of till. Quaternary International, **18**: 97–101. doi:10.1016/1040-6182(93)90057-M.
Stoops, G., and Jongerius, A. 1975. A proposal for a micromorphological classification of soil materials. I. A classification of the related distributions of fine and coarse particles. Geoderma, **13**(3): 189–199. doi:10.1016/0016-7061(75)90017-8.
Stow, D.A.V., and Aksu, A.E. 1978. Disturbances in soft sediments due to piston coring. Marine Geology, **28**(1–2): 135–144. doi:10.1016/0025-3227(78)90101-9.
Studinger, M., Bell, R.E., and Tikku, A.A. 2004. Estimating the depth and shape of subglacial Lake Vostok's water cavity from aerogravity data. Geophysical Research Letters, **31**(12). doi:10.1029/2004GL019801.
Sturm, A., and Matter, A. 1978. Turbidites and varves in Lake Brienz (Switzerland): deposition of clastic detritus by density currents. *In* Modern and ancient lake sediments. *Edited by* A. Matter and M.E. Tucker. International Association of Sedimentologists, Special publication. pp. 147–168. doi:10.1002/9781444303698.
Tikku, A.A., Bell, R.E., Studinger, M., Clarke, G.K.C., Tabacco, I., and Ferraccioli, F. 2005. Influx of meltwater to subglacial Lake Concordia, East Antarctica. Journal of Glaciology, **51**(172): 96–104. doi:10.3189/172756505781829494.
van der Meer, J.J.M. 1993. Microscopic evidence of subglacial deformation. Quaternary Science Reviews, **12**: 553–587. doi:10.1016/0277-3791(93)90069-X.
van der Meer, J.J.M., and Menzies, J. 2011. The micromorphology of unconsolidated sediments. Sedimentary Geology, **238**(3–4): 213–232. doi:10.1016/j.sedgeo.2011.04.013.
van der Meer, J.J.M., and Warren, W.P. 1997. Sedimentology of late glacial clays in lacustrine basins, central Ireland. Quaternary Science Reviews, **16**: 779–791. doi:10.1016/S0277-3791(97)00022-X.
van der Meer, J.J.M., Carr, S.J., and Kjær, K.H. 2010. Mýrdalsjökull's forefields under the microscope. The Micromorphology of meltout and subglacial tills. Developments in Quaternary Science, **13**: 159–180. doi:10.1016/S1571-0866(09)01310-4.
van der Wateren, F.M., Kluiving, S.J., and Bartek, L.R. 2000. Kinematic indicators of subglacial shearing. *In* Deformation of glacial materials. *Edited by* A.J. Maltman, B. Hubbard and M.J. Hambrey. Geological Society, London, Special publications, vol. 176. pp. 259–278. doi:10.1144/GSL.SP.2000.176.01.20.
Wingham, D.J., Siegert, M.J., Shepherd, A., and Muir, A.S. 2006. Rapid discharge connects Antarctic subglacial lakes. Nature, **440**: 1033–1036. doi:10.1038/nature04660. PMID:16625193.
Wright, A., and Siegert, M. 2012. A fourth inventory of Antarctic subglacial lakes. Antarctic Science, **24**(6): 659–664. doi:10.1017/S095410201200048X.